REFERENCES

[1] M. A Stuchly, S S. Stuchly, and G. Kantor, "Diathermy applicators with circular aperture and corrugated flange," *IEEE Trans. Microwave Theory Tech.*, vol. MTT-28, pp 267–271, Mar 1980.

[2] M E J. Jeuken, M H. M. Knoben, and K. J. Wellington, "A dual frequency, dual polarised feed for radio astronomical applications," *Nachrichtentech. Z.*, vol. 25, pp. 374–376, 1972

[3] R Wohlleben, H. Mattes, and O. Lochner, "Simple small primary feed for large opening and high aperture efficiency," *Electron. Lett.*, vol. 8, pp. 474–476, 1972

[4] C. A. Balanis, "Pattern distortions due to edge diffractions," *IEEE Trans. Antennas Propagat.*, vol. AP-18, pp. 561–563, July 1970.

[5] R. E. Lawrie and L Peters, Jr., "Modifications of horn antennas for low side-lobe levels," *IEEE Trans. Antennas Propagat.*, vol. AP-14, pp. 605–610, Sept. 1966.

[6] P. S Neelakantaswamy and D. K. Banerjee, "Circular waveguide aperture with a curved corrugated disk as a primary feed," in Dig. Int IEEE/G-AP Symp USNC/URSI Meet. (Boulder, CO), 1973, pp. 228–231

[7] P. S Neelakantaswamy and D. K. Banerjee, "Radiation characteristics of a circular waveguide aperture with a curved disk," *Arch. Elekt. Ubertragung.*, vol 28, pp. 277–279, June 1974.

[8] P S. Neelakantaswamy, "A circular waveguide primary feed with a corrugated concave disk at its aperture," *Z. elektr Inform.-u. Energietecknik*, vol. 5, pp. 356–361, May 1975.

[9] P. S. Neelakantaswamy, "Studies on open-ended circular waveguide radiators with modified aperture-ends," Ph D. thesis, Electrical Eng. Dept., Ind. Inst. of Tech., Madras, India, Sept. 1975.

[10] M. C. Bailey and C. T. Swift, "Input admittance of a circular waveguide aperture covered by a dielectric slab," *IEEE Trans. Antennas Propagat.*, vol. AP-16, pp. 386–391, July 1968.

[11] R C. Rudduck and C. L Yu, "Circular waveguide method for measuring reflection properties of absorber panels," *IEEE Trans. Antennas Propagat.*, vol. AP-22, pp. 251–256, Mar. 1974

[12] C M. Knop and H. J. Wiesenfarth, "On the radiation from an open-ended corrugated pipe carrying the HE_{11} mode," *IEEE Trans. Antennas Propagat.*, vol. AP-20, pp. 644–648, Sept. 1972.

[13] P S. Neelakantaswamy, K. K. Gupta, and D. K. Banerjee, "A Gaussian-beam launcher for microwave exposure studies," *IEEE Trans. Microwave Theory Tech* , vol. MTT-25, pp 426–428, May 1977.

[14] _____, "Field aberrations in the focal region of a microwave gaussian-beam launcher," *Arch. Elek. Übertragung.*, vol. 32, pp. 85–87, Feb. 1978.

[15] _____, "Near-field characteristics of a scalar horn-fed dielectric spherical radiator," *Arch. Elek. Übertragung.*, vol. 31, pp. 173–175, Apr. 1977.

[16] P. S Neelakantaswamy and F. C Hong, "Design of a microwave Gaussian-beam launcher with prescribed constraints on its beam characteristics," *Arch Elek. Ubertragung.*, vol. 33, pp. 174–177, Apr. 1979.

[17] P. S Neelakantaswamy and F. C. Hong, "Dielectric hemisphere-loaded scalar horn as a Gaussian-beam launcher for microwave exposure studies," *IEEE Trans. Microwave Theory Tech.*, vol. MTT-27, pp. 797–799, Sept. 1979.

Microwave Power Absorption in a Biological Specimen Inside a Standing-Wave Irradiation Waveguide

OSAMU FUJIWARA AND YOSHIFUMI AMEMIYA

***Abstract*—An irradiation system consisting of a standing-wave in a waveguide is a convenient way to study biological effects of the individual components of the microwave fields. This paper describes microwave power absorption in a biological specimen exposed to standing waves inside the waveguide with a reflection plate. A method is presented to obtain the absorbed power distribution and total power absorption in a prolate spheroidal model of a specimen having small dimensions compared to the guide wavelength. Numerical results on the pupa of Tenebrio molitor are given, and also verified experimentally.**

Manuscript received March 30, 1982; revised June 15, 1982.

The authors are with the Department of Electrical Engineering, Faculty of Engineering, Nagoya University, Furo-cho, Chikusa-ku, Nagoya 464, Japan.

I. INTRODUCTION

In investigating biological effects and potential hazards of electromagnetic (EM) radiation, many detailed theoretical analyses of the EM power absorption in various tissue-equivalent models have recently been performed. In this type of analysis, either plane-wave irradiation in free space [1]–[5] or traveling-wave exposure in waveguide [6], [7] has usually been considered, and thus electric and magnetic fields were assumed to interact simultaneously with the biological tissue.

Of particular interest here are interactions of individual electric and magnetic field components of microwave fields with the tissue, for which no theoretical analyses have previously been made.

In order to investigate separately the effects of the electric and magnetic fields on biological specimens such as animal, insect, bacteria, etc., a standing-wave irradiation waveguide system is convenient. This paper presents a method for calculating the absorbed power density and total absorbed power in such specimens modeled as prolate spheroids inside the waveguide with a reflection plate, when the guide wavelength is long compared to the spheroidal dimensions.

Numerical calculations on the Tenebrio pupa, which has often been used to study the microwave biological effects [8]–[11], are given as an example, and the results are compared with experimental measurements.

II. THEORY

A. Standing-Wave Irradiation Waveguide

Fig. 1 shows a standing-wave irradiation system using a rectangular waveguide. Biological specimens are mounted in styrofoam and inserted along the center line of the waveguide at half intervals of a guide wavelength λ_g.

In terms of the rectangular coordinates shown in Fig. 1, standing-wave fields inside the empty waveguide which operates in TE_{10} mode can be written by

$$\begin{aligned}\mathbb{E}_s &= (-j2E_f)\cos(\pi x/a)\sin\left[2\pi(z-d)/\lambda_g\right] \\ &\quad \cdot \exp(j\omega t - j2\pi d/\lambda_g)\hat{y} \\ \mathbb{H}_s &= (-2E_f/\eta_0)(\lambda/\lambda_g)\cos(\pi x/a) \\ &\quad \cdot \cos\left[2\pi(z-d)/\lambda_g\right]\exp(j\omega t - j2\pi d/\lambda_g)\hat{x} \\ &\quad + (-2E_f/\eta_0)(\lambda/2a) \\ &\quad \cdot \sin(\pi x/a)\sin\left[2\pi(z-d)/\lambda_g\right]\exp(j\omega t - j2\pi d/\lambda_g)\hat{z}\end{aligned}$$

where $\mathbb{E}_s$ and $\mathbb{H}_s$ are electric and magnetic field vectors, respectively. η_0 is the free-space intrinsic impedance, λ is the free-space wavelength, and ω is the angular frequency. E_f represents the amplitude of the incident electric field, which can be calculated simply from $E_f = 2\sqrt{(\lambda_g/\lambda)(P_f \cdot \eta_0/ab)}$ where P_f is a forward power into the waveguide. $\hat{x}$, $\hat{y}$, and $\hat{z}$ are the unit vectors in the x, y, and z directions, respectively.

When the biological specimen has dimensions small enough compared to the guide wavelength λ_g and the waveguide width a, the specimen placed at the origin is exposed to the following

0018-9480/82/1100-2008$00.75 ©1982 IEEE

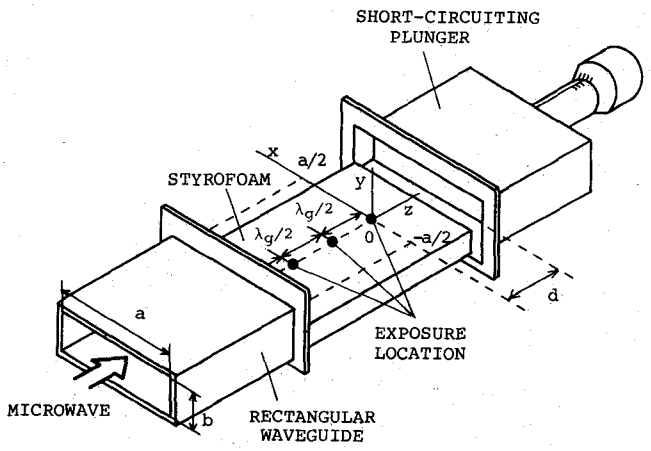

Fig. 1. Standing-wave irradiation waveguide.

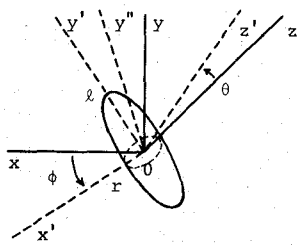

Fig. 2. Prolate spheroidal model of biological specimen and its coordinate systems.

uniform electromagnetic fields:

$$\mathbb{E}_s = E_s\hat{y} = (j2E_f)\sin(2\pi d/\lambda_g)\exp(j\omega t - j2\pi d/\lambda_g)\hat{y}$$

$$\mathbb{H}_s = H_s\hat{x} = (-2E_f/\eta_0)(\lambda/\lambda_g)\cdot\cos(2\pi d/\lambda_g)\exp(j\omega t - j2\pi d/\lambda_g)\hat{x}. \quad (1)$$

B. Microwave Power Absorption

Fig. 2 shows a prolate spheroidal model of the biological specimen and its rectangular coordinate systems.

The coordinate system of $0\text{-}x'y'z'$ in which the y'-axis coincides with the major axis of the spheroid is chosen here. This system is obtained by rotating a system of $0-xy''z'$ counterclockwise to an angle ϕ on the z'-axis, where the $0-xy''z'$ system is given by a left-handed rotation of the $0-xyz$ system to an angle θ on the x-axis. Then, the relationship between the coordinates of (x, y, z) and (x', y', z') can be formulated as

$$\begin{bmatrix} x \\ y \\ z \end{bmatrix} = \begin{bmatrix} \cos\phi & \sin\phi & 0 \\ -\cos\theta\cdot\sin\phi & \cos\theta\cdot\cos\phi & \sin\theta \\ \sin\theta\cdot\sin\phi & -\sin\theta\cdot\cos\phi & \cos\theta \end{bmatrix} * \begin{bmatrix} x' \\ y' \\ z' \end{bmatrix}. \quad (2)$$

From (2), the standing-wave fields of (1) can be changed in terms of the system $0\text{-}x'y'z'$ into

$$\mathbb{E}_s = E_s(-\cos\theta\cdot\sin\phi\hat{x}' + \cos\theta\cdot\cos\phi\hat{y}' + \sin\theta\hat{z}') \quad (3)$$

$$\mathbb{H}_s = H_s(\cos\phi\hat{x}' + \sin\phi\hat{y}') \quad (4)$$

where x', y', and z' are the unit vectors parallel to the coordinate axes of the $0-x'y'z'$.

In order to obtain internal electric fields in the prolate spheroid exposed to the standing-waves of (3) and (4), quasi-static approaches developed by Durney *et al.* [2] and Shiau and Valentino [12] could be applied independently.

Assuming that the spheroid consists of homogeneous material with a complex relative permittivity $\epsilon_r = \epsilon_{r'} - j\epsilon_{r''}$ and a free-space permeability μ_0, quasi-static solutions are given by

$$\mathbb{E}_e = E_s(-U_h\sin\theta\cdot\sin\phi\hat{x}' + U_e\cos\theta\cdot\cos\phi\hat{y}' + U_h\sin\theta\hat{z}')$$

$$\mathbb{E}_h = j\omega\mu_0 H_s\{-(z'/2)\sin\phi\hat{x}' + (u_0^2/2u_0^2 - 1)z'\sin\phi\hat{y}' + [(x'/2)\sin\phi - (u_0^2 - 1/2u_0^2 - 1)y'\sin\phi]\hat{z}'\}$$

where

$$U_e = 1/\{1 + (\epsilon_r - 1)(u_0^2 - 1)[u_0\coth^{-1}(u_0) - 1]\}$$

$$U_h = 1/\{1 + (1 - \epsilon_r)(u_0/2)[(u_0^2 - 1)\coth^{-1}(u_0) - u_0]\}$$

$$u_0 = l/\sqrt{l^2 - r^2}.$$

$\mathbb{E}_e$ and $\mathbb{E}_h$ represent internal electric fields induced electrically by (3) and magnetically by (4), respectively. A total internal electric field $\mathbb{E}$ is given by a sum of the above quasi-static solutions, i.e., $\mathbb{E} = \mathbb{E}_e + \mathbb{E}_h$.

A time-average absorbed power density P which represents the absorbed power distribution in the spheroid can be calculated from

$$P = (\sigma/2)|E|^2 \quad (5)$$

where σ is a conductivity of the spheroid denoted as $\sigma = \omega\epsilon_0\epsilon_{r''}$ (ϵ_0: free-space permittivity).

A time-average absorbed power P_a (that is, the total absorbed power) is given by the volumetric integral: $P_a = \int_V P dv$, which can be reduced to

$$\frac{P_a}{P_f} = \frac{16\pi\epsilon_{r''}}{\sqrt{1-(\lambda/2a)^2}}\frac{V}{ab\lambda}\left\{\left[|U_h|^2\cos^2\theta\cdot\sin^2\phi + |U_e|^2\cos^2\theta\cdot\cos^2\phi + |U_h|^2\sin^2\theta\right]\sin^2(2\pi d/\lambda_g) + \frac{1}{5}\left(\frac{2\pi}{\lambda_g}\right)^2 \cdot\left(\frac{1}{2}r^2\sin^2\phi + \frac{l^2r^2}{l^2+r^2}\cos^2\phi\right)\times\cos^2(2\pi d/\lambda_g)\right\} \quad (6)$$

where V is the spheroidal volume $V = 4\pi lr^2/3$.

C. Numerical Calculations

In order to give numerical calculations on the microwave power absorption described above, consider a pupa of Tenebrio molitor shown in Fig. 3, which has often been used in experiments for microwave irradiation studies [8]–[11].

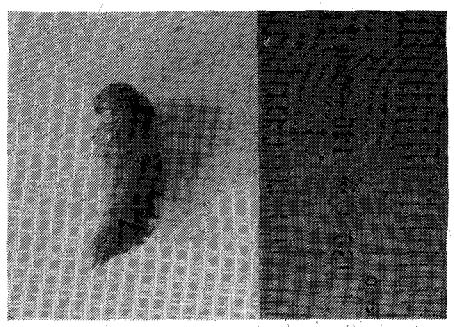

Fig. 3. Pupa of Tenebrio molitor.

A typical pupa has a 15-mm length and a 5-mm diameter with a mass of 150 mg. The exposure electromagnetic field is taken as 2-GHz band microwave, the wavelength of which is long enough compared to the pupal dimensions. Thus, the waveguide unit considered here is WRJ-2 (equivalent WR-430) waveguide with $a = 10.922$ cm and $b = 5.461$ cm in cross section, which is de-

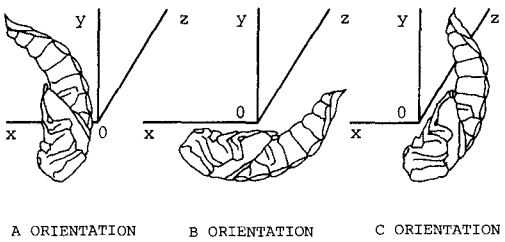

Fig. 4. Pupa orientations for exposure.

signed to operate in the TE_{10} mode within the frequency range of 1.7–2.6 GHz.

Fig. 4 shows the three primary orientations of the pupa for exposure in the waveguide, whose definitions are as follows. The A and B orientations are obtained in Fig. 2 by $\theta = \phi = 0$, $\theta = 0$, and $\phi = \pi/2$, respectively. The pupae placed in these orientations are exposed to electric and magnetic fields in parallel with the pupal major axes, respectively. The C orientation is given in Fig. 2 by $\theta = \pi/2$ and $\phi = 0$. In this case, both the electric and magnetic field vectors are perpendicular to the major axis of the pupa.

The relative permittivity at a given frequency for the Tenebrio pupa might be estimated under the assumption that the pupal permittivity has the same kind of Debye-type dispersion characteristics that body tissues have [13].

Using the values of $\epsilon_r = 30 - j18$ at 9 GHz measured by Lindauer *et al.* [9] and Schwan's equations that express well the electrical properties of nearly all body tissues with high water content [14], the relative permittivity $\epsilon_r = \epsilon_{r'} - j\epsilon_{r''}$ as a function of frequency for the pupa can be expressed by

$$\epsilon_{r'} = 5 + 30/\left[1 + (f/f_0)^2\right]$$

$$\epsilon_{r''} = 13 + 30 \times (f/f_0)^2/\left[1 + (f/f_0)^2\right] \qquad (7)$$

where $f_0 = 20$ GHz.

Fig. 5 shows numerical values of the total power absorption in the pupa simulated by the prolate spheroid placed in each exposure orientation of Fig. 4, which were calculated from (6). The ordinate shows the total absorbed power in the spheroid normalized to the forward power into the waveguide. Notice that the 2-GHz band microwave power absorbed by the spheroid is extremely small compared to the forward waveguide power.

Fig. 5(a) shows the power absorption due to the electric field given by $d = (2n+1)\lambda_g/4$ in (1) where n is a nonnegative integer. As seen from the figure, the exposure in the A orientation causes the highest power absorption in the spheroid. This can be explained qualitatively by the electric field coupling to the spheroid [2], which is strongest in the A orientation because of the field boundary conditions such that the tangential electric field must be continuous at the spheroidal surface.

Fig. 5(b) shows the power absorption due to the magnetic field given by $d = n\lambda_g/2$ ($n \neq 0$) in (1). Note that the magnetic field exposure in all orientations causes smaller power absorption than the electric field exposure. It is found in Fig. 5(b) that the exposure in the B orientation causes the lowest power absorption in the spheroid. This is qualitatively because the spheroid in the B orientation intercepts less magnetic flux than those in the A and C orientations [2].

Fig. 6 shows numerical values of the absorbed power density along the x, y, and z axes of the spheroid, which were calculated from (5). The ordinate shows the relative absorbed power density in the spheroid normalized to the total absorbed power per unit

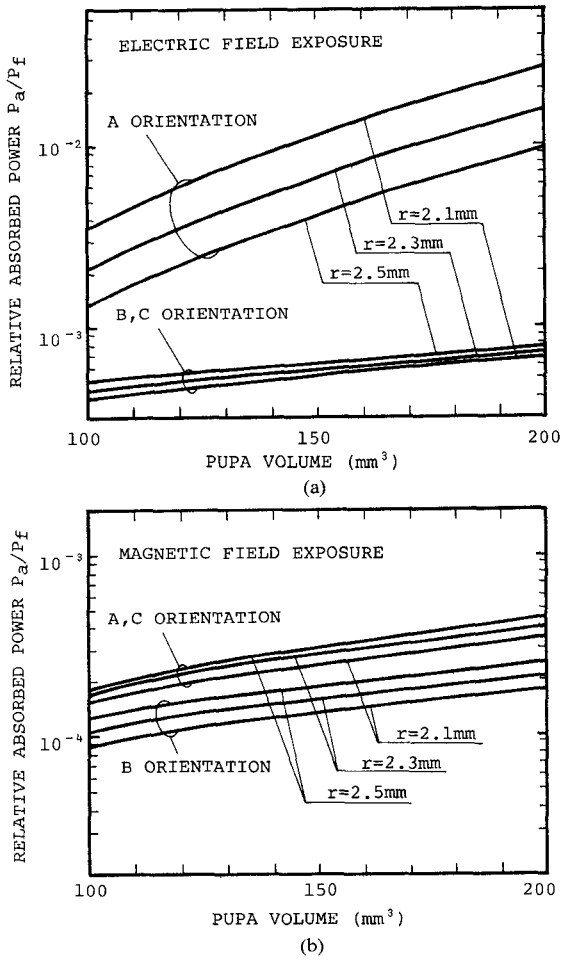

Fig. 5 Calculated 2450-MHz microwave power absorption in pupa simulated by a prolate spheroid exposed to (a) electric field and (b) magnetic field. Relative permittivity calculated for the pupa is $\epsilon_r = 35 - j13$ at 2450 MHz.

volume of the spheroid. Notice that the absorbed power density and the total absorbed power can be controlled independently by the distance from the spheroid to the shorting plunger and by the forward waveguide power, respectively.

The dotted lines of Fig. 6 show the cases of the spheroid exposed to the electric field. The broken curves show the cases of the spheroid exposed to both the electric and magnetic fields, the magnitudes of which are $\sqrt{2}$ times larger than those in the case of the traveling-wave irradiation inside a terminated waveguide. The solid curves show the cases of the spheroid exposed to the magnetic field.

The calculated results in the case of $d/\lambda_g = 0.375$ are qualitatively similar to those on the spheroid irradiated by plane waves, which were obtained by Johnson *et al.* [15]. However, the results in other cases are quite different.

As seen from Fig. 6, the absorbed power density in the case of $d/\lambda_g = 0.250$ is uniform inside the spheroid and thus the electric field exposure causes the homogeneous heating in the spheroid. On the other hand, in the case of $d/\lambda_g = 0.500$, the absorbed power density is significantly small in the vicinity of the origin inside the spheroid and high on the spheroidal surface. Thus, the magnetic field exposure causes the inhomogeneous heating similar to the conventional caloric heating.

It is concluded from the above results that the 2-GHz band standing-wave fields significantly produce the different absorbed power distributions, which might cause the different biological

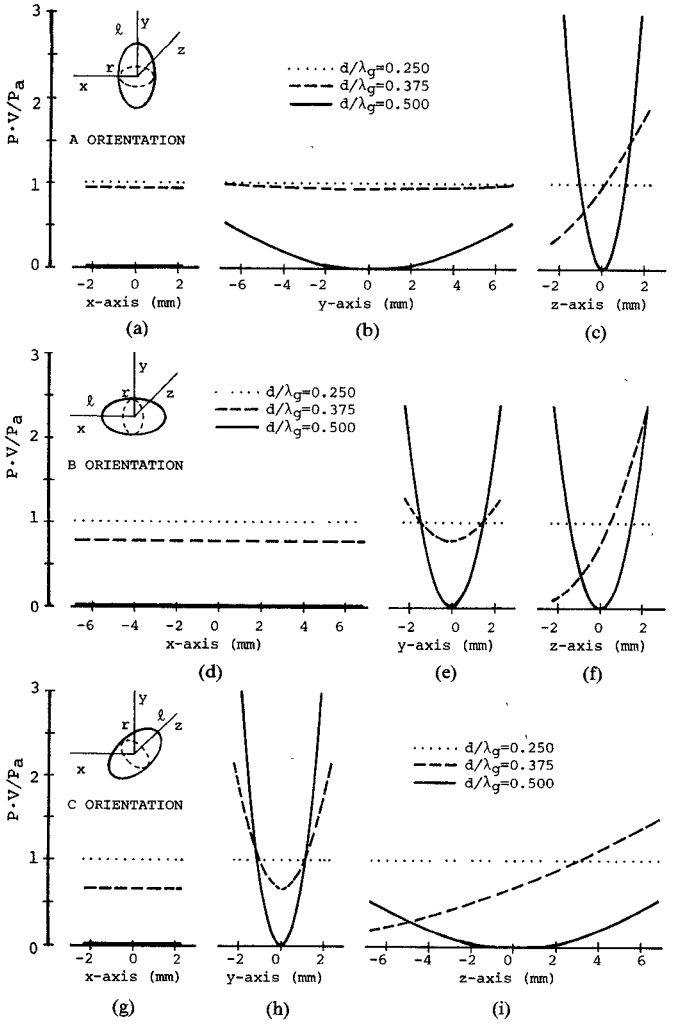

Fig. 6. Calculated spatial distribution of 2450-MHz microwave power absorption in a pupa equivalent to a prolate spheroid with $l = 6.8$ mm and $r = 2.3$ mm ($V = 150$ mm^3).

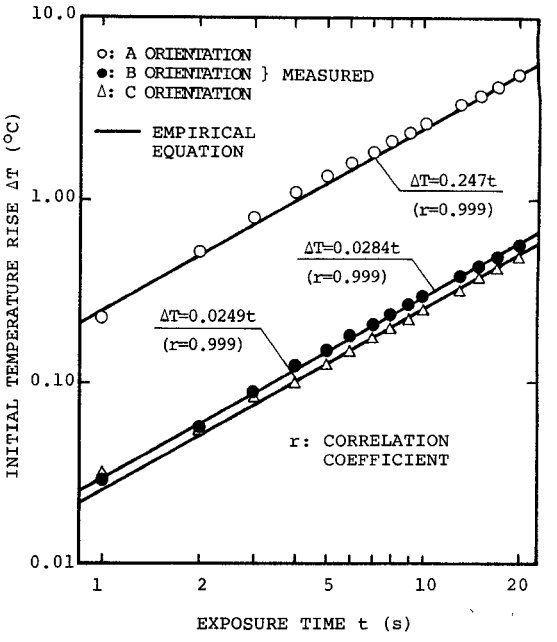

Fig. 7. Measurements of initial temperature rise in pupa exposed to the electric field given by $d/\lambda_g = 0.75$. Pupa mass = 157 mg, $f = 2485$ MHz, $P_f = 10$ W.

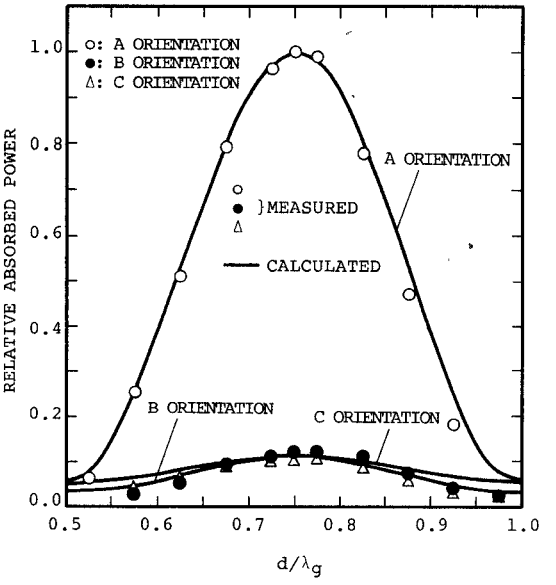

Fig. 8. Relative absorbed power in pupa exposed to standing-wave fields. Pupa mass = 157 mg, $f = 2485$ MHz, $P_f = 10$ W.

effects on the pupa, even though the total absorbed powers due to each exposure field are all the same.

III. Experiments

A. Experimental Method

In order to confirm the numerical results described in the previous section, experiments on the 2-GHz band microwave exposure are carried out by using the standing-wave irradiation waveguide as shown in Fig. 1. The waveguide unit used was the WRJ-2 waveguide. One-day-old living pupae were chosen for exposure samples.

The total power absorbed by the pupa is obtained by measuring the gradient of an initial temperature rise due to the exposure standing-wave. The temperature rise is monitored by imbedding a fine chromelalumel thermocouple (diameter: 76 μmϕ) in the abdomen of the sample pupa. Exposure of the thermocouple itself to the standing-waves inside the waveguide produces no measurable temperature rise, since the lead wires are placed perpendicularly to the electric field vector.

B. Results and Discussion

Fig. 7 shows measurements of the initial temperature rise in the pupa exposed to the electric field given by $d/\lambda_g = 0.75$. The solid lines shows empirical equations that express the measured temperature rise ΔT, which were obtained by a least-squares method.

The initial temperature rise of Fig. 7 can be assumed to be the same at all points inside the pupa because of the uniform absorbed power density. Thus, the total absorbed power P_a can be given by

$$P_a = mC(d\Delta T/dt) \tag{8}$$

where m is a pupa mass and C is a specific heat of the pupa.

In the case of the magnetic field exposure, (8) is not valid because the absorbed power density is highly nonuniform. However, under the assumption that the thermal time constant of the pupa is sufficiently small compared to the exposure time, (8)

would also be applicable to the case of the magnetic field exposure.

Fig. 8 shows experimental results on the total power absorption in the pupa exposed to the standing waves. The ordinate shows the relative absorbed power which is obtained from (8) by normalizing the measured value of the $d\Delta T/dt$ to that in the A-oriented pupa of Fig. 7. The abscissa shows the relative distance from the pupa to the shorting plunger normalized to the guide wavelength. The solid curves show the values of the relative absorbed power calculated from (6), which approximately agree with the experimental results.

As regards the parameters for calculations, the pupa mass $m = 157$ mg and the pupa diameter $2r = 4.8$ mm were both measured. The pupa length $l = 6.5$ mm was obtained from $l = 3m/4\pi\rho r^2$ where ρ is a density of the sample pupa assumed to be 1 mg/mm^3. The relative permittivity $\epsilon_r = 35 - j13$ at the experimental frequency $f = 2485$ MHz was calculated from (7).

IV. Conclusions

The microwave power absorption in the biological specimen modeled as the prolate spheroid inside the standing-wave irradiation waveguide has been examined theoretically with respect to the exposure orientation.

The absorbed power distribution and total power absorption in the spheroid with dimensions small compared to the guide wavelength were obtained in simple closed form expressions.

Numerical calculations on the Tenebrio pupa were presented, and the results on the total power absorption were confirmed experimentally.

References

[1] A R Shapiro, R. F. Lutomirski, and H T Yura, "Induced fields and heating within a cranial structure irradiated by an electromagnetic plane wave," *IEEE Trans. Microwave Theory Tech.*, vol. MTT-19, pp 187–196, Feb. 1971.

[2] C H Durney, C C. Johnson, and H. Massoudi, "Long wavelength analysis of plane-wave irradiation of a prolate spheroid model of man," *IEEE Trans. Microwave Theory Tech.*, vol. MTT-23, pp 246–253, Feb. 1975.

[3] H. Massoudi, C H. Durney, and C. C. Johnson, "Long wavelength analysis of plane wave irradiation of an ellipsoidal model of man," *IEEE Trans. Microwave Theory Tech.*, MTT-25, pp 41–46, Jan. 1977.

[4] T K. Wu and L. L. Tsai, "Electromagnetic fields induced inside arbitrary cylinders of biological tissue," *IEEE Trans. Microwave Theory Tech.*, vol. MTT-25, pp 61–65, Jan. 1977.

[5] K. M. Chen and B. S. Guru, "Internal EM field and absorbed power density in human torsos induced by 1–500-MHz EM waves," *IEEE Trans Microwave Theory Tech.*, vol. MTT-25, pp 746–756, Sept. 1977

[6] L. M. Liu, F. J. Rosenbaum, and W. F. Pickard, "Electric-field distribution along finite length lossy dielectric slabs in waveguide," *IEEE Trans. Microwave Theory Tech.*, vol. MTT-24, pp. 216–219, Apr. 1976

[7] R. G. Olsen, G. A. Geithan, and D. H. Schrader, "A microwave irradiation chamber for scientific studies on agricultural products," *IEEE Trans. Microwave Theory Tech.*, vol. MTT-25, pp. 428–433, May 1977.

[8] R. L. Carpenter and E. M. Livstone, "Evidence for nonthermal effects of microwave radiation: Abnormal development of irradiated insect pupae," *IEEE Trans Microwave Theory Tech.*, vol. MTT-19, pp. 173–178, Feb. 1971.

[9] G. A. Lindauer, L M. Liu, G. W. Skewes, and F. J. Rosenbaum, "Further experiments seeking evidence of nonthermal effects of microwave radiation," *IEEE Trans. Microwave Theory Tech*, vol. MTT-22, pp. 790–793, Aug. 1974

[10] L. M Liu, F J Rosenbaum, and W. F. Pickard, "The relation of teratogenesis in Tenebrio molitor to the incidence of low-level microwaves," *IEEE Trans. Microwave Theory Tech.*, vol. MTT-22, pp. 790–793, Aug. 1974

[11] R. G. Olsen, "Insect teratogenesis in a standing-wave irradiation system," *Radio Sci.*, vol. 12(6S), pp. 199–207, 1977.

[12] Y Shiau and A. R. Valentino, "ELF electric field coupling to dielectric spheroidal models of biological objects," *IEEE Trans. Bio-Med. Eng.*, vol. BME-28, pp. 429–437, June 1981

[13] S. O. Nelson and L F. Charity, "Frequency dependence of energy absorption by insects and grain in electric fields," *Trans. ASAE.*, vol 15, pp. 1099–1102, Nov. 1972.

[14] H. P. Schwan, "Interaction of microwave and radio frequency radiation with biological systems," *IEEE Trans. Microwave Theory Tech.*, vol. MTT-19, pp. 146–152, Feb. 1971.

[15] C C. Johnson, C. H. Durney, and H. Massoudi, "Long-wavelength electromagnetic power absorption in prolate spheroidal models of man and animals," *IEEE Trans. Microwave Theory Tech.*, vol. MTT-23, pp 793–747, Sept. 1975.

Comparison of AM Noise from a Klystron and an IMPATT Oscillator at around 90 GHz

G. A. EDISS, N. J. KEEN, AND P. ZIMMERMAN

***Abstract*—This paper reports comparisons between the amplitude modulation noise performance of a Plessey IMPATT oscillator AT0273 and a Varian VRB-2113 klystron at millimeter wavelengths.**

I. Introduction

Millimeter-wave radiometers require stable sources of local-oscillator (LO) power, with low amplitude modulation (AM) noise levels at $f_{LO} \pm f_{IF}$. The frequency modulation (FM) and AM noise close to the carrier is also important, but within approximately 1 MHz of the carrier this can be greatly reduced by the use of phase lock loops (PLL) [1], but the use of a PLL will have no effect upon the oscillator noise outside this range. The presence and effect of such AM noise far from the carrier has been demonstrated by Cong and Kerr [2] who showed that the AM noise-to-carrier ratio of a doubled 57-GHz klystron was equal or better than that of three klystrons operating between 110 and 114 GHz, and by Tearle and Heath [3] who showed the effect of sideband noise of IMPATT pumps on parametric amplifier noise temperatures.

Recent advances in IMPATT diode technology to increase power capability, lifetime[1], and the use of high-Q waveguide circuits to reduce the noise of these devices (see, for example, Gokgor *et al.* [4], Berson and Kuno [5], and Bischoff and Schroth [6]) suggest that IMPATT oscillators can replace klystrons as local oscillators at frequencies up to 100 GHz.

II. The Measurements

The double sideband noise temperature of a low-noise mixer was measured using the standard hot-and-cold load technique [7]. As shown in Fig. 1, the local oscillator was coupled into the mixer through a directional coupler, and two waveguide resonant-ring filters were used to further reduce the far-from-carrier noise. The filters were successively removed and the system noise temperature was measured with room temperature and liquid nitrogen loads in front of the horn, and with a noise source

Manuscript received March 23, 1982; revised June 4, 1982. This work was supported in part by the Deutsche Forschungsgemeinschaft, (SFB 131).

The authors are with the Max-Planck-Institut fur Radioastronomie, Auf dem Hugel 69, D-5300 Bonn, West Germany

[1]For example W. J Welch (private communication) reports more than 15000 h continuous operation of two phase-locked IMPATT local oscillators on the 86-GHz interferometer of the University of California (Berkeley)

0018-9480/82/1100-2012$00.75 ©1982 IEEE